Inverse Control of Systems with Hysteresis and Creep

Pavel Krejci[*)] , Klaus Kuhnen[!)]

[*)] Weierstraß-Institut for Applied Analysis and Stochastics (WIAS)

Mohrenstraße 39, 10117 Berlin, Germany

[!)] Saarland University, Laboratory for Process Automation (LPA)

Im Stadtwald Building 13, 66041 Saarbrücken, Germany

Abstract

Since the beginning of the 1990s hysteresis operators have been employed on a larger scale for the linearisation of hysteretic transducers. One reason for this is the increasing number of mechatronic applications which use solid-state actuators based on magnetostrictive or piezoelectric material or shape memory alloys. All of these actuator types show strong hysteretic effects. In addition to hysteresis, piezoelectric actuators show strong creep effects. Thus, the objective of this article is to enlarge the operator-based methodology of the hysteresis operators by elements that allow the description of systems with hysteresis and creep. To reach this objective, following the procedure used for hysteretic systems, creep operators are introduced to form, together with the hysteresis operators, the system operator for the simultaneous consideration of both phenomena. With regard to applications in control and measurement technology the existence, the uniqueness, the Lipschitz continuity and thus the input-output stability of its inverse operator are theoretically supported by functional analytical methods. Subsequently, the efficiency of this new concept is demonstrated in practice by a real-time inverse feedforward controller for piezoelectric actuators. Using this control concept, the tracking errors caused by hysteretic and creep effects are reduced by approximately one order of magnitude.

1. Introduction

Models for the description of hysteretic transducers have evolved from two different branches of physics: ferromagnetism and plasticity theory. The roots of both branches go back to the end of the 19th century. But only at the beginning of the 1970s a mathematical formalism for a systematic consideration of hysteretic transducers was developed. The core of this theory is formed by so-called hysteresis operators which describe hysteretic transducers as a mapping between function spaces. From this approach an autonomous branch within system theory has developed starting with the fundamental work of the Russian mathematicians M.A. Krasnosel'skii and A.V. Pokrovskii; their approach makes it possible to consider complex hysteretic transfer characteristics in a purely phenomenological way without taking into account the underlying physics.

But it is only since the beginning of the 1990s that engineers employ this theory on a larger scale to develop modern strategies for the linearisation of hysteretic systems. One reason for this is the increasing number of mechatronic applications in the last years which use new solid-state actuators based on magnetostrictive or piezoelectric material or shape memory alloys. All of these actuator types show strong hysteretic effects. Whereas in the beginning mainly the Preisach operator was used for the modeling and control of solid-state actuators [1]-[3], recent papers also use the Prandtl-Ishlinskii operator, in particular for the mathematical description and control of piezoelectric actuators [4]-[6].

Besides the hysteresis effects, the transfer characteristic of piezoelectric actuators also shows dynamic creep effects that are not to be ignored. Although this is known since a long time and is explicitly investigated in [1], up to now this fact has been neglected in the concepts for modeling and control. However, as hysteresis operators due to their nature are static transducers, the simultaneous consideration of hysteresis and creep requires an enlargement of the operator-based concept by elements for the description of such dynamic effects. In the past this kind of enlargement of the Preisach operator has been elaborated by Mayergoyz, Bertotti and Kortendieck [7]-[9]. These approaches, however, have in common that the models are not suited for a practical concept of a real-time inverse feedforward controller for the simultaneous compensation of hysteresis and creep because of the great computational costs for calculation and identification.

Thus, the objective of this article is to enlarge the operator-based methodology of the hysteresis operators by elements that allow the description of systems with hysteresis and creep. This will be done in Section 2. With regard to applications in control and measurement technology, it is important to prove the existence and the uniqueness of the operator being inverse to the system operator, because the proof represents the theoretical precondition for the success of the inversion processes to realize an inverse feed-forward controller or an inverse filter for the compensation of the nonidealities introduced by hysteresis and creep effects. The theorems of existence, uniqueness and Lipschitz continuity and thus the input-output stability of the inverse operator are the object of section 3 whereas the proofs of these properties are moved to the appendix. In Section 4 an efficient numerical implementation of the inverse operator is presented. Finally, in section 5 the performance of the method is demonstrated in practice by an inverse feedforward controller for the compensation of hysteresis and creep phenomena in the transfer characteristic of piezoelectric actuators.

In comparison to a conventional feedback controller the main advantages of this operator-based inverse feedforward controller are that the compensation of hysteretic nonlinearities and creep dynamics is also achieved under highly dynamic operation and that no additional sensor for the system output is used for compensation purposes. This leads to a very simple and inexpensive control system for the optimization of such mechatronic devices. The main drawback of the inverse feedforward controller is the sensitivity to unconsidered external disturbances which are introduced for example by temperature dependence. If such effects play a role in a specific application the combination of inverse feedforward and feedback control paradigms leads to a controller with optimized performance both for the static and for the dynamic behaviour of the overall system.

2. Operator-based Hysteresis and Creep Modeling

Let $C[0,T]$ denote the space of continuous functions $u{:}[0,T] \to \mathrm{R}$ endowed with the norm $||u||_\infty := \max\{|u(t)|; t \in [0,T]\}$, where $T > 0$ is a given number. We consider the operator $F{:}C[0,T] \to C[0,T]$ given by the formula

$$F[u](t) := au(t) + \int_0^\infty b(r) p_r[\pi_0, u](t)\,dr + \int_0^\infty c(\lambda) l_\lambda[\xi_0, u](t)\,d\lambda \tag{1}$$

where *a* is a given constant, *b* and *c* are given functions with the properties

(i) $a > 0,\ b(r) \geq 0$ and $c(\lambda) \geq 0$ a.e. (*almost everywhere*),

(ii) $b(r),\ c(\lambda) \in L^1(0,\infty)$ and $L_C := \int_0^\infty \lambda c(\lambda) \mathrm{d}\lambda < \infty$.

p_r and l_λ are the elementary hysteresis and linear creep operators defined in the following way. Here the abbreviations $\dot{u}(t) = \frac{\mathrm{d}}{\mathrm{d}t} u(t)$ and $\pi'(r) = \frac{\mathrm{d}}{\mathrm{d}r} \pi(r)$ are used.

Definition 1.1

(i) *Let* Π *denote the space of functions* $\pi : [0,\infty[\to R$ *which are Lipschitz continuous,* $|\pi'(r)| \leq 1$ *a.e., and there exists some* $R > 0$ *such that* $\pi(r) = 0$ *for* $r \geq R$. *For a given function* $\pi_0 \in \Pi$, *a given number* $r > 0$ *and a given function* $u \in C[0,T]$ *we define the play operator* $p_r : \Pi \times C[0,T] \to C[0,T]$ *with threshold r as the solution operator* $p_r[\pi_0, u](t) := z_r(t)$ *of the rate-independent hybrid differential equation*

$$\dot{z}_r(t) = \begin{cases} \dot{u}(t) & \text{if} \quad z_r(t) - r = u(t) \\ 0 & \text{if} \quad z_r(t) - r < u(t) < z_r(t) + r \\ \dot{u}(t) & \text{if} \quad z_r(t) + r = u(t) \end{cases} \tag{2}$$

with the initial value equation

$$z_r(0) = \max\{u(0) - r, \min\{u(0) + r, \pi_0(r)\}\}.$$

(ii) *For a given function* $\xi_0 \in L^\infty(0,\infty)$, *a given number* $\lambda > 0$ *and a given function* $u \in C[0,T]$ *we define the linear creep operator* $l_\lambda : L^\infty(0,\infty) \times C[0,T] \to C^1[0,T]$ *with the eigenvalue* λ *as the solution operator* $l_\lambda[\xi_0, u](t) := z_\lambda(t)$ *of the differential equation*

$$\frac{1}{\lambda} \dot{z}_\lambda(t) + z_\lambda(t) = u(t) \tag{3}$$

with the initial value equation

$$z_\lambda(0) = \xi_0(\lambda)\ .$$

We actually have the explicit integral formula

$$l_\lambda[\xi_0, u](t) = e^{-\lambda t} \xi_0(\lambda) + \lambda \int_0^t e^{\lambda(\tau - t)} u(\tau)\, \mathrm{d}\tau \tag{4}$$

for the operator l_λ. The linear creep operator is mainly characterized by its so-called creep eigenvalue λ which determines the dynamic properties of this elementary system, see figure 2. The play operator

however is mainly characterized by its threshold parameter r which determines the width of the hysteresis region in the z_r,u-plane, see figure 3. The spaces Π and $L^\infty(0,\infty)$ are the state spaces for the operator (1). A mechanical interpretation of the operator F defined by (1) can be given in terms of the constitutive law $\varepsilon = F[\sigma]$, where ε and σ are the uniaxial strain and stress, respectively. The formula in (1) corresponds to the rheological diagram shown in Fig. 4 below. The individual, parallel linear viscoelastic elements to the right correspond to the linear creep operators l_λ, while the parallel elastoplastic elements to the left represent the play operators p_r. Hence the first term in (1) describes the linear reversible part, the second term describes the hysteretic part and the third term describes the creep part of systems with hysteresis and creep.

3. Input-Output Stability of the Inverse Operator

From the control point of view the aim of this section is to show that the operator F is invertible in $C[0,T]$ and both F and its inverse F^{-1} are Lipschitz continuous and thus input-output stable in $C[0,T]$. For this purpose we decompose the operator (1) into a purely rate-independent part

$$P[u](t) := au(t) + \int_0^\infty b(r)\, p_r[\pi_0, u](t)\, dr \tag{5}$$

and a purely rate-dependent part

$$L[u](t) := \int_0^\infty c(\lambda)\, l_\lambda[\xi_0, u](t)\, d\lambda. \tag{6}$$

After a few conversions of (1) we obtain the implicit operator equation

$$u(t) = P^{-1}[w - L[u]](t) \tag{7}$$

with the output $w(t) = F[u](t)$ which contains the inverse of the rate-independent operator P. The inverse F^{-1} of the operator F is defined as the solution operator of the implicit operator equation (7) which can be regarded as the basic law for the design of inverse feedforward controllers. Figure 5 shows the feedback structure of the inverse operator F^{-1}. Now we have to show that this solution operator exists, is unique and Lipschitz continuous and thus input-output stable under the constraints described by the properties of a, b and c. To do this we first recall some well-known properties of the purely rate-independent operator (5) called Prandtl-Ishlinskii operator. The following results can be found in Chapter 2 of [11] or section II.3 of [13].

Theorem 1.3

(i) *For every* $u, v \in C[0,T]$, $t \in [0,T]$ *and* $r > 0$ *we have*

$$|p_r[\pi_0, u](t) - p_r[\pi_0, v](t)| \leq \max_{0 \leq \tau \leq t} |u(\tau) - v(\tau)| \tag{8}$$

(ii) *For* $r > 0$ *put*

$$\begin{aligned} &\varphi(r) := ar + \int_0^r b(\varsigma)(r-\varsigma)\mathrm{d}\varsigma\,, \\ &\hat{a} := \frac{1}{a}\,, \\ &\hat{b}(r) := (\varphi^{-1})''(r)\,, \\ &\hat{\pi}_0(r) := -\int_{\varphi^{-1}(r)}^{\infty} \pi_0'(\varsigma)\varphi'(\varsigma)\mathrm{d}\varsigma\,, \end{aligned} \tag{9}$$

where φ^{-1} *is the inverse function to* φ. *Then the inverse operator* P^{-1} *to* P *is also a Prandtl-Ishlinskii operator and is given by the formula*

$$P^{-1}[u](t) := \hat{a}u(t) + \int_0^{\infty} \hat{b}(r)\, p_r[\hat{\pi}_0, u](t)\, dr\,. \tag{10}$$

By definition, the function φ is convex and $\varphi''(r) = b(r)$ a.e., hence φ^{-1} is concave and $\hat{b}(r) \leq 0$ a.e. As a direct consequence of Thm. 1.3, we see that both P^{-1} and P are causal and Lipschitz continuous in $C[0,T]$. We denote by $L_{P^{-1}}$ the Lipschitz constant of P^{-1} that is,

$$\begin{aligned} L_{P^{-1}} &:= \hat{a} + \int_0^{\infty} |\hat{b}(r)|\, dr = \hat{a} - \int_0^{\infty} (\varphi^{-1})''(r) dr = \hat{a} - (\varphi^{-1})'(\infty) + (\varphi^{-1})'(0) \\ &= \hat{a} - \frac{1}{\varphi'(\infty)} + \frac{1}{\varphi'(0)} = \frac{2}{a} - \frac{1}{a + \int_0^{\infty} b(r) dr} \end{aligned}\,. \tag{11}$$

With the above properties of P^{-1} the following theorem shows that the operator F is a bijection of $C[0,T]$ onto $C[0,T]$.

Theorem 1.4

For every $w \in C[0,T]$ *there exists a unique* $u \in C[0,T]$ *such that* $w = F[u]$.

To conclude this section, it remains to mention that also F^{-1} is Lipschitz continuous with constant $L_{P^{-1}} e^{L_{P^{-1}} L_C T}$ and thus input-output stable in $C[0,T]$.

Theorem 1.5

Under the above hypotheses, we have for every $u, v \in C[0,T]$

$$\|u-v\|_\infty \le L_{P^{-1}} e^{L_{P^{-1}} L_C T} \|F[u]-F[v]\|_\infty . \tag{12}$$

The proofs are the object of the appendix.

4. Numerical Implementation of the Inverse Operator

To calculate the compensation signal in real-time a digital signal processor (DSP) is used. Therefore a time-discrete model for the operator *F* is developed. Using a rectangular approximation for the numerical calculation of the integral equation (4), we obtain a simple first-order difference equation

$$z_\lambda(k+1) = e^{-\lambda T_s} \cdot z_\lambda(k) + (1 - e^{-\lambda T_s}) \cdot u(k) \tag{13}$$

with the initial value $z_\lambda(0) = \xi_0$ and

$$l_\lambda[\xi_0, u](k) = z_\lambda(k) \tag{14}$$

as a time-discrete counterpart to the time-continuous elementary creep operator. In equation (13) T_s is the sampling time. The output sequence of the discrete play operator can be calculated by the difference equation analogous to (2):

$$z_r(k) = \begin{cases} u(k) + r & , \text{ if } z_r(k-1) - r \ge u(k) \\ z_r(k-1) & , \text{ if } z_r(k-1) - r < u(k) < z_r(k-1) + r \\ u(k) - r & , \text{ if } z_r(k-1) + r \le u(k) \end{cases} \tag{15}$$

with the initial value $z_r(0) = \max\{u(0) - r, \min\{u(0) + r, \pi_0(r)\}\}$ and

$$p_r[\pi_0, u](k) = z_r(k) \ . \tag{16}$$

In practice due to the continuity property of the play operator complex continuous hysteresis loops can be modeled in a sufficiently precise way with a small number of elementary operators [14]. Analogously real visco-elastic creep phenomena can be modeled in a sufficiently precise way with a small number of elementary linear creep operators [15]. Therefore the operator (1) is replaced by the finite sum version

$$F[u](k) := au(k) + \sum_{i=1}^{n} b_i p_{r_i}[\pi_0, u](k) + \sum_{j=1}^{m} c_j l_{\lambda_j}[\xi_0, u](k) \tag{17}$$

for the practical realization of the inverse feedforward controller. (17) is a special case of (1) which follows from the choice

$$b(r) := \sum_{i=1}^{n} b_i \delta(r - r_i) \quad \text{and} \quad c(\lambda) := \sum_{j=1}^{m} c_j \delta(\lambda - \lambda_j)$$

for the functions $b(r)$ and $c(\lambda)$ with the Dirac distribution δ, $0 < r_1 < \ldots < r_n < \infty$ and $0 < \lambda_m < \ldots < \lambda_1 < \infty$. In this case the properties of a, *b* and *c* are reduced to

(i) $0 < a < \infty$, $0 \le b_i < \infty$ and $0 \le c_j < \infty$.

The problem of finding the inverse control value $u(k)$ for a given control value $w_c(k)$ and thus to obtain the inverse operator F^{-1} is equivalent to the solution of the implicit operator equation (7) in the discrete-time case. Because of the fact that the output $L[u](k)$ at the time point *k* depends only on the states $z_{\lambda_1}(k-1),..,z_{\lambda_m}(k-1)$ of the rate-dependent part and on $u(k-1)$, see (13), we can calculate $u(k)$ by (7) if the controller input $w_c(k)$, the output $L[u](k)$ and the inverse operator P^{-1} are known. After the calculation of $u(k)$ the output $L[u](k+1)$ of the rate-dependent part can be updated for the next time step. To obtain the inverse operator

$$P^{-1}[u](k) := \hat{a}u(k) + \sum_{i=1}^{n} \hat{b}_i p_{\hat{r}_i}[\hat{\pi}_0, u](k) \tag{18}$$

we have to calculate the thresholds $\hat{r}_1,..,\hat{r}_n$, the weights $\hat{a}$ and $\hat{b}_1,..,\hat{b}_n$ and the initial memory state $\hat{\pi}_0$. In this case, the function φ from Theorem 1.3 (ii) is convex and piecewise affine, and its derivative φ' has the form

$$\varphi'(r) = a + \sum_{i=1}^{j} b_i \quad \text{for} \quad r \in [r_j, r_{j+1}[\ , \ j = 0, \ldots, n, \tag{19}$$

where we put $r_0 := 0$, $r_{n+1} := \infty$. Its inverse φ^{-1} is therefore affine in each interval $[\hat{r}_l, \hat{r}_{l+1}[$ for $l = 0, \ldots, n$ where $\hat{r}_l = \varphi(r_l)$, $l = 0, \ldots, n$ and in particular $\hat{r}_0 = 0$, $\hat{r}_{n+1} = \infty$. This yields that

$$\hat{r}_l = \hat{r}_{l-1} + \int_{r_{l-1}}^{r_l} \varphi'(r)\, \mathrm{d}r = \hat{r}_{l-1} + (a + \sum_{i=1}^{l-1} b_i)(r_l - r_{l-1}) \tag{20}$$

for $l = 1, \ldots, n$. Summing up the identities (20) over *l* from 1 to *j* we obtain

$$\hat{r}_j = \sum_{l=1}^{j} (a + \sum_{i=1}^{l-1} b_i)(r_l - r_{l-1}) = a r_j + \sum_{i=1}^{j-1} \sum_{l=i+1}^{j} b_i (r_l - r_{l-1}) = a r_j + \sum_{i=1}^{j-1} b_i (r_j - r_i) \ , \tag{21}$$

which is nothing more than the desired inversion formula for the thresholds. To compute the weights corresponding to the inverse operator, we observe that in each interval $[\hat{r}_j, \hat{r}_{j+1}[$ for $j = 0, \ldots, n$ we have

$$\varphi^{-1}(r) = \hat{a} + \sum_{i=1}^{j} \hat{b}_i = \frac{1}{a + \sum_{i=1}^{j} b_i} \ , \tag{22}$$

hence, in particular,

$$\hat{a} = \frac{1}{a} \ , \tag{23}$$

and

$$\hat{b}_j = -\frac{b_j}{(a+\sum_{i=1}^{j} b_i)(a+\sum_{i=1}^{j-1} b_i)} \tag{24}$$

for $j = 1, \ldots, n$. It remains to derive an expression for the initial state $\hat{\pi}_0$. Indeed, only its values at the points $\hat{r}_1, .., \hat{r}_n$ are relevant. By Theorem 1.3 (ii) we have for $j = 1, \ldots, n$

$$\begin{aligned}
\hat{\pi}_0(\hat{r}_j) &= -\int_{\varphi^{-1}(\hat{r}_j)}^{\infty} \pi_0'(r)\varphi'(r)\mathrm{d}r = -\int_{r_j}^{\infty} \pi_0'(r)\varphi'(r)\mathrm{d}r \\
&= -\sum_{l=j}^{n} \int_{r_l}^{r_{l+1}} \pi_0'(r)(a+\sum_{i=1}^{l} b_i)\mathrm{d}r = -\sum_{l=j}^{n} (\pi_0(r_l)-\pi_0(r_{l+1}))(a+\sum_{i=1}^{l} b_i). \\
&= (a+\sum_{i=1}^{j} b_i)\pi_0(r_j) + \sum_{l=j+1}^{n} b_l \pi_0(r_l)
\end{aligned} \tag{25}$$

The above formulae and the rate independence property guarantee that the operator (18) is inverse to the discrete-threshold version of the Prandtl-Ishlinskii operator (5).

5. Inverse Feedforward Controller for a Piezoelectric Actuator

To test the compensation method presented above, a micropositioning stage based on a piezoelectric stack actuator as a driving element was realized. Fig. 6 illustrates the test and measurement equipment of the experimental part. It consists of a digital signal processor (DSP) which generates the digital driving signal for the piezoelectric actuator. This signal is converted by a 12-bit digital-to-analog converter and amplified by an high-voltage power amplifier to an analog high-voltage signal of up to 1 kV. The output of the high-voltage power amplifier is measured by an additional voltage measurement circuit and converted to a digital signal by a 12-bit analog-to-digital converter. The displacement of the actuator is directly digitally measured by a high-precision laser-interferometer with a resolution of 5 nm. The signals from the voltage measurement circuit and the interferometer are fed back to the DSP for characterization, identification and control purposes. The measured relation between the driving voltage signal, see Fig. 7a, and the displacement signal of the actuator in the large signal range, see Fig. 7b, is shown in Fig. 7c. Caused by creep effects the displacement signal changes with time although the input signal is constant, compare Fig. 7a and 7b. Therefore the hysteresis loops in Fig 7c contain vertical jumps which are characteristic for rate-dependent phenomena as they cannot be described by rate-independent operators. To model the hysteretic and creep transfer characteristic of the piezoelectric actuator the time-discrete version of the operator F was comprised of $n = 6$ play operators with fixed threshold values r_i which are determined by

$$r_i = \frac{i}{n+1}\|u\|_\infty \quad ; \quad i = 1 \,..\, n \tag{26}$$

with $\|u\|_\infty = 1$ in this normalized case and of m = 5 elementary linear creep operators with fixed eigenvalues λ_j which are determined by

$$\lambda_j = \frac{1}{10^{j-1} T_s} \quad ; \quad j = 1 \,..\, m \tag{27}$$

with a sampling period of T_s = 1 ms in this application. The free parameters c_j, b_i and a were identified using nonlinear optimization procedures to minimize the deviation between the normalized measured and modeled transfer characteristics under the contraints, see Tab. 1. Apart from the measurement values, which are shown as a dashed line in Fig. 7b and Fig. 7c, these figures also show the output-input chracteristic calculated on the basis of the operator F as a solid line. Fig. 7d finally shows the error signal e between the real system response and the one calculated by the operator F as a solid line as well as the error signal e between the real system response and the one calculated by a linear characteristic as a dashed line. While the maximum value of the error signal e reaches up to 8.6 % of the range of the displacement signal when compared to a linear characteristic, the operator F reduces these value to 0.82 %. This corresponds to an improvement of more than one order of magnitude.

To verify the performance of the inverse control procedure, the compensator was implemented on a DSP TMS 320C40 and driven with an input signal $w_c(t)$ shown in Fig. 8a. The calculation time of the compensator is less than 0.1ms and so a sampling frequency up to 10 kHz is possible. Fig. 8b shows the output signal of the compensator. This signal shows the inverse characteristic of the displacement signal in Fig. 7b. Due to the compensation the actuator output signal is nearly free of hysteretic and creep effects, see Fig. 8c. Fig. 8d presents the measured output-input characteristic of the serial connection of the compensator and the real system. Due to the compensation effect of the inverse operator the vertical lines and the branching caused by the creep and hysteresis phenomena are strongly reduced. In the case of the inverse feedforward control paradigm the relative deviation of the transfer characteristic from an optimal linear characteristic, which is caused by the model error, amounts to only 1%.

6. Conclusions

The main contribution of this paper consists in introducing a combined complex operator which is used for modeling of systems with hysteresis and creep. The proof of existence, uniqueness, Lipschitz continuity and thus input-output stability of the inverse operator are natural preconditions for the practical realisation of the inverse operator via a numerical inversion procedure. The performance of the operator-based method is practically demonstrated by means of a compensator for a micropositioning stage based on a piezoelectric stack actuator. It is experimentally shown that the tracking error of the stage is reduced by one order of magnitude. In future works we will extend the method on the one hand by visco-plastic type elementary creep operators to improve the creep modeling and on the other hand by nonlinear superposition operators to model unsymmetrical characteristics like saturation phenomena in systems with hysteresis and creep.

Acknowledgement

The authors thank the Deutsche Forschungsgemeinschaft (DFG), the Weierstraß Institute for Applied Analysis and Stochastics (WIAS) and the Laboratory for Process Automation at the Saarland University (LPA) for the financial and nonfinancial support of this work.

References

[1] GE, P.; JOUANEH, M.: 'Generalized Preisach model for hysteresis nonlinearity of piezoceramic actuators', *Precision Engineering*, 1997, **20** pp. 99-111

[2] LAST, B.; HEROLD-SCHMITT, U.; BAIER, H.: 'Active Structures with Hysteresis Actuators: Linearization Techniques and Correlation with Test Results', 7th Int. Conf. Adaptive Structures Technology, ICAST'96, 1996, Rome, Italy

[3] SCHÄFER, J.; JANOCHA, H.: 'Compensation of hysteresis in solid state actuators', *Sensors and Actuators Physical A*, 1995, **49** pp. 97-102

[4] GOLDFARB, M.; CELANOVIC, N.: 'Modeling Piezoelectric Stack Actuators for Control of Micromanipulation', *IEEE Control Systems*, 1997, pp. 69-79

[5] DIMMLER, M.; HOLMBERG, U.; LONGCHAMP, R.: 'Hysteresis Compensation of Piezo Actuators', European Control Conference, ECC'99, 1999, Karlsruhe, Germany

[6] KUHNEN, K.; JANOCHA, H.: 'Adaptive inverse control of piezoelectric actuators with hysteresis operators', European Control Conference, ECC'99, 1999, Karlsruhe, Germany

[7] MAYERGOYZ, I.D.: 'Mathematical Models of Hysteresis' (Springer-Verlag, New York, 1991)

[8] BERTOTTI, G.: 'Dynamic generalization of the scalar Preisach model of hysteresis', *IEEE Trans. Magn.*, 1992, **28** (5) pp. 2599-2601

[9] KORTENDIECK, H.: 'Entwicklung und Erprobung von Modellen zur Kriech- und Hysteresiskorrektur' (VDI- Verlag, Düsseldorf, 1993)

[10] JANOCHA, H.; KUHNEN, K.: 'Ein neues Hysterese- und Kriechmodell für piezoelektrische Wandler', *at-Automatisierungstechnik*, 1998, **46** pp. 493-500

[11] BROKATE, M.; SPREKELS, J.: 'Hysteresis and Phase Transitions' (Springer-Verlag, Berlin-Heidelberg-NewYork, 1996)

[12] KRASNOSEL'SKII, M. A.; POKROVSKII, A. V.: 'Systems with Hysteresis' (Springer-Verlag, Berlin, 1989)

[13] KREJCI, P.: 'Hysteresis, Convexity and Dissipation in Hyperbolic Equations', *Gakuto Int. Series Math. Sci. & Appl.*, 1996, **8**, Gakkotosho, Tokyo

[14] BERGQVIST, A.: 'On magnetic hysteresis modeling', Electric Power Engineering, Royal Institute of Technology Stockholm, 1994.

[15] KUHNEN, K.; JANOCHA, H.: 'Compensation of Creep and Hysteresis Effects of Piezoelectric Actuators with Inverse Systems', 6th Int. Conf. on New Actuators, Actuator'98, 1998, Bremen, Germany, p. 309-312

Appendix

Our aim is to prove that the operator F is invertible in $C[0,T]$ and both F and its inverse F^{-1} are Lipschitz continuous.

Proof of Theorem 1.4

For every $u,v \in C[0,T]$ we have by (4) for every $\lambda > 0$ and $t \in [0,T]$

$$|l_\lambda[\xi_0,u](t) - l_\lambda[\xi_0,v](t)| \le \lambda \int_0^t |u(\tau) - v(\tau)| \mathrm{d}\tau \,. \tag{28}$$

Let $w \in C[0,T]$ be given and let $\Gamma : C[0,T] \to C[0,T]$ be the operator

$$\Gamma[x](t) := w(t) - \int_0^\infty c(\lambda) l_\lambda[\xi_0, P^{-1}[x]](t) d\lambda \tag{29}$$

According to (29), we have for all $x,y \in C[0,T]$

$$|\Gamma[x](t) - \Gamma[y](t)| \le L_C \int_0^t |P^{-1}[x](\tau) - P^{-1}[y](\tau)| d\tau \le L_{P^{-1}} L_C \int_0^t \max_{0\le\rho\le\tau} |x(\rho) - y(\rho)| d\tau \,, \tag{30}$$

hence also

$$\max_{0\le\rho\le t} |\Gamma[x](\rho) - \Gamma[y](\rho)| \le L_{P^{-1}} L_C \int_0^t \max_{0\le\rho\le\tau} |x(\rho) - y(\rho)| d\tau \,. \tag{31}$$

From the above inequality it immediately follows that the n-th iterate Γ^n of Γ satisfies

$$\max_{0\le\rho\le t} |\Gamma^n[x](\rho) - \Gamma^n[y](\rho)| \le L_{P^{-1}} L_C \int_0^t \max_{0\le\rho\le\tau} |\Gamma^{n-1}[x](\rho) - \Gamma^{n-1}[y](\rho)| d\tau \tag{32}$$

for every $t \in [0,T]$ and $n \ge 1$, with the convention $\Gamma^0[x] = x$ and $\Gamma^0[y] = y$. By induction we conclude that

$$\max_{0\le\rho\le t} |\Gamma^n[x](\rho) - \Gamma^n[y](\rho)| \le \frac{(L_{P^{-1}} L_C t)^n}{n!} ||x - y||_\infty \tag{33}$$

for every $t \in [0,T]$ and $n \ge 1$. For n sufficiently large, the mapping Γ^n is therefore a contraction in $C[0,T]$. According to the Banach Contraction Principle, Γ admits a unique fixed point $x \in C[0,T]$, that is, $\Gamma[x] = x$. It suffices to put $u := P^{-1}[x]$ and the proof is complete.

The Lipschitz continuity of F follows immediately from (8) and (28). It remains to prove Theorem 1.5 which implies that also F^{-1} is Lipschitz continuous with constant $L_{P^{-1}} e^{L_{P^{-1}} L_C T}$.

Proof of Theorem 1.5

Let $u, v \in C[0,T]$ be given. We proceed as in the Proof of Thm. 1.4 putting $x := P[u]$, $y := P[v]$. Then we have

$$F[u]-F[v] = x-y+\int_0^\infty c(\lambda) l_\lambda[\xi_0, P^{-1}[x]-P^{-1}[y]]d\lambda , \tag{34}$$

hence

$$|x(t)-y(t)| \le ||F[u]-F[v]||_\infty + L_{P^{-1}} L_C \int_0^t \max_{0\le\rho\le\tau} |x(\rho)-y(\rho)| d\tau \quad . \tag{35}$$

The Gronwall lemma yields

$$\max_{0\le\tau\le t} |x(\tau)-y(\tau)| \le e^{L_{P^{-1}} L_C t} ||F[u]-F[v]||_\infty \ . \tag{36}$$

for every $t \in [0,T]$ and Thm. 1.5 is proved.

a	0.5806
b_1	0.1443
b_2	0.0539
b_3	0.0204
b_4	0.0208
b_5	0.0032
b_6	0.0002
c_1	0.0693
c_2	0.0722
c_3	0.0582
c_4	0.0694
c_5	0.0478

Tab. 1: Weights of the operator F

Fig. 1: Inverse feedforward controller for hysteretic and creep systems

Fig. 2: Dynamic characteristic of the linear creep operator

Fig. 3: Rate-independent transfer characteristic of the play operator

Fig. 4: The rheological structure of the operator F

Fig 5: Signal flow chart of the inverse operator

Fig 6: Test- and measurement equipment for a piezoelectric micropositioning stage

Fig. 7: Actuator reaction $y(t)$ versus the input-signal $u(t)$ and model error $e(t)$:

a) Input signal $u(t)$ b) System reaction $w(t)$

c) Output-input-trajectory $w(u)$ d) Model error $e(t)$

Fig. 8: Results of the inverse control process:

a) Given control signal $w_c(t)$ b) Compensator output signal $u(t)$ c) Actuator output signal $w(t)$

d) Actuator output signal $w(t)$ versus the given control signal $w_c(t)$

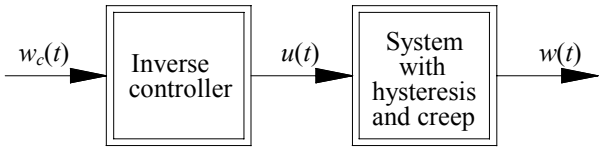
$w_c(t)$
Inverse controller
$u(t)$
System with hysteresis and creep
$w(t)$

Fig.1

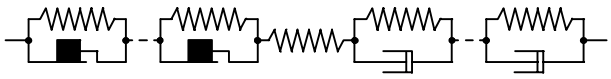

Fig.4

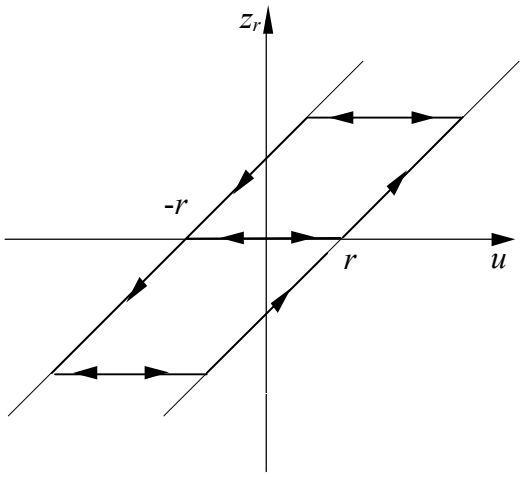

Fig.3

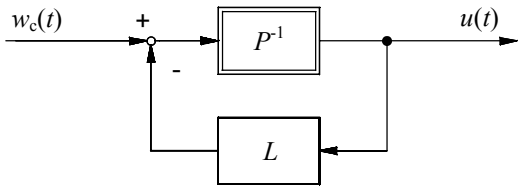

Fig.5

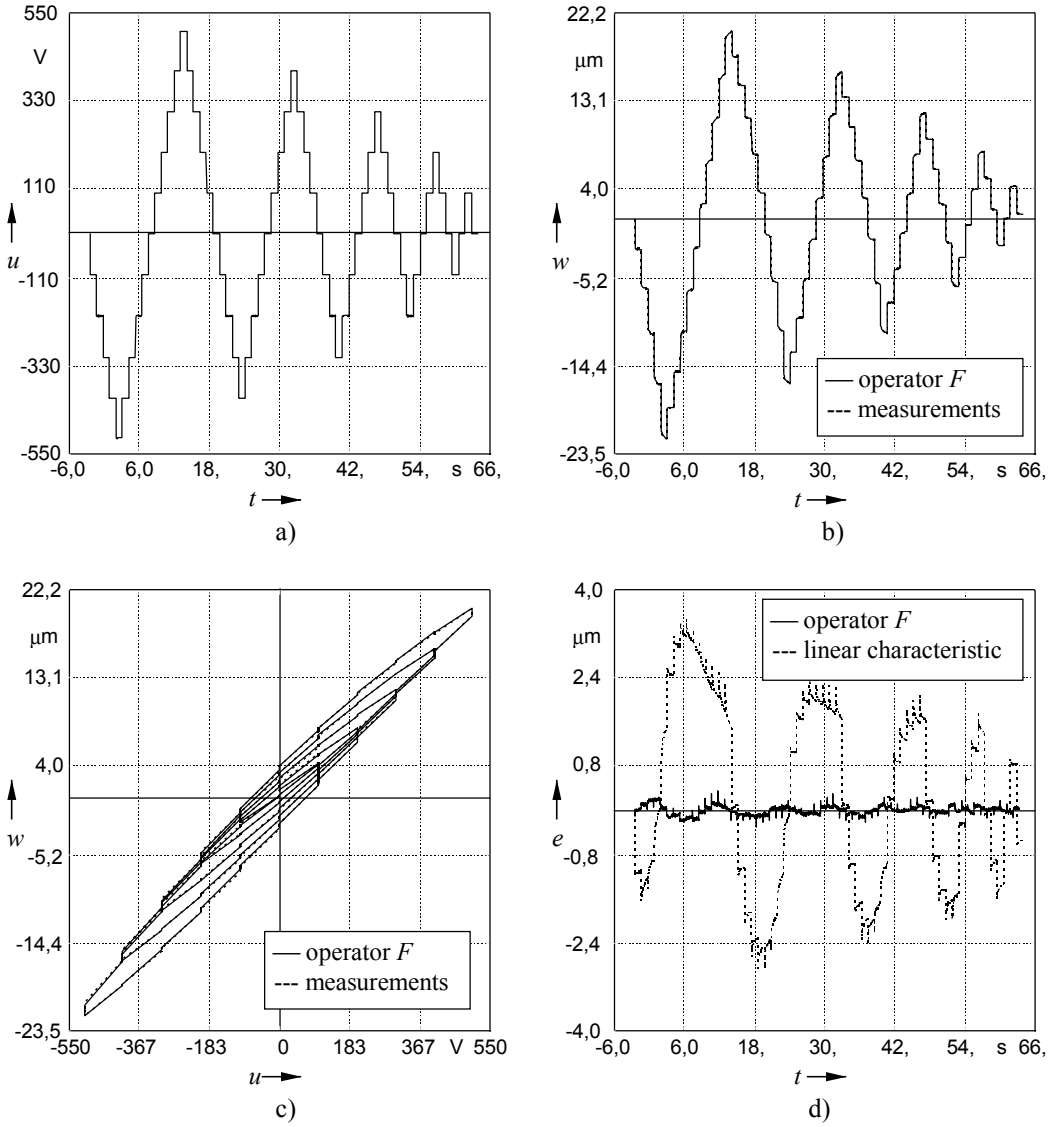
550
V
330
110
u
-110
-330
-550
-6,0
6,0
18,
30,
42,
54,
s 66,
t
a)
22,2
μm
13,1
4,0
w
-5,2
-14,4
-23,5
— operator F
--- measurements
b)
c)
— operator F
--- linear characteristic
4,0
2,4
0,8
e
-0,8
-2,4
-4,0
d)

Fig. 7

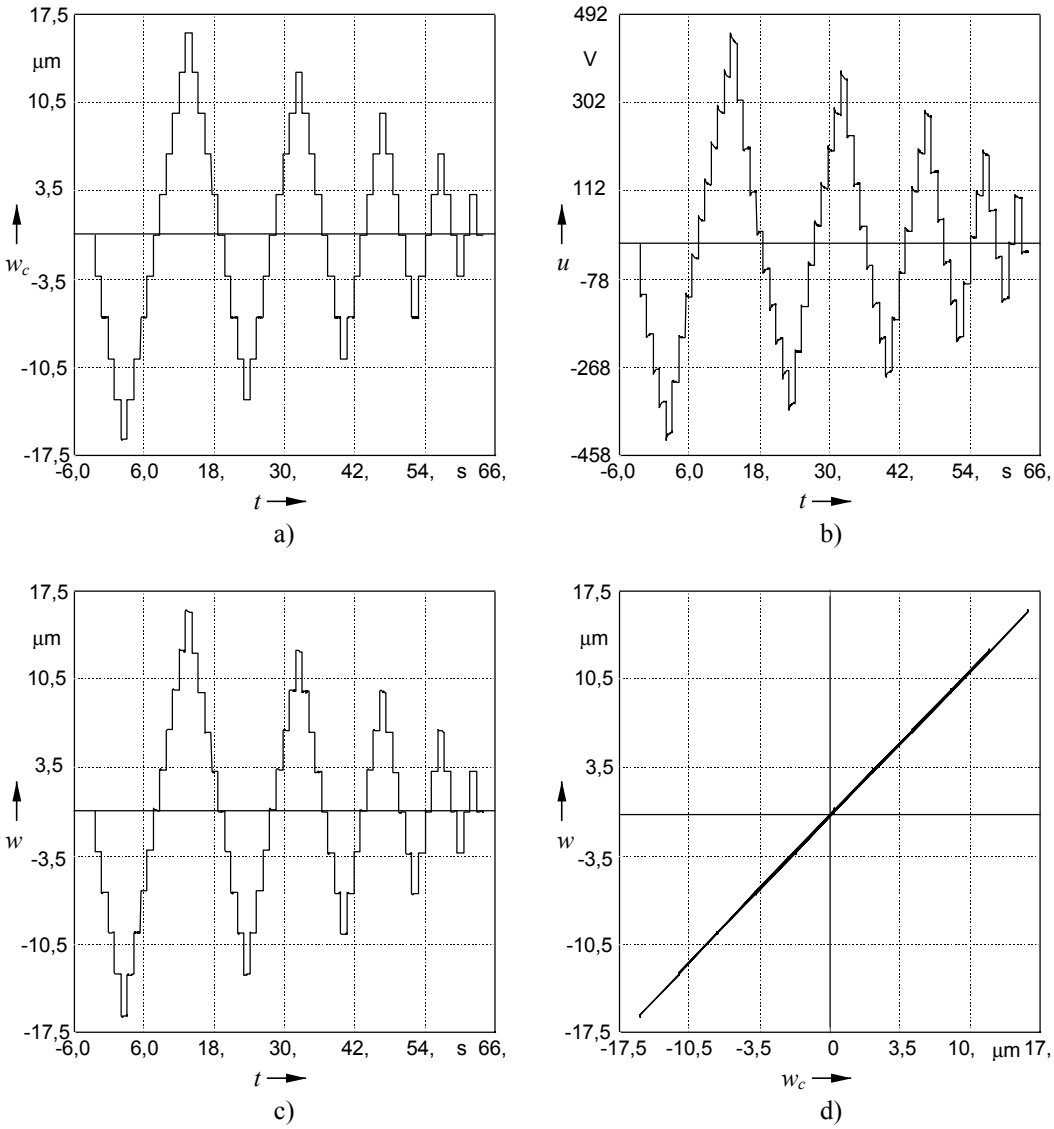
17,5
µm
10,5
3,5
w_c
-3,5
-10,5
-17,5
-6,0
6,0
18,
30,
42,
54,
s 66,
t
a)
492
V
302
112
u
-78
-268
-458
-6,0
6,0
18,
30,
42,
54,
s 66,
t
b)
17,5
µm
10,5
3,5
w
-3,5
-10,5
-17,5
-6,0
6,0
18,
30,
42,
54,
s 66,
t
c)
17,5
µm
10,5
3,5
w
-3,5
-10,5
-17,5
-17,5
-10,5
-3,5
0
3,5
10,
µm 17,
w_c
d)

Fig.8

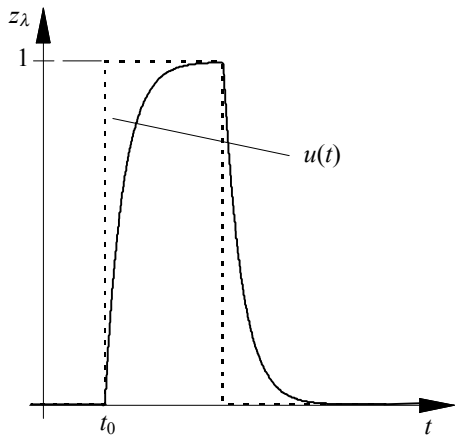

Fig. 2

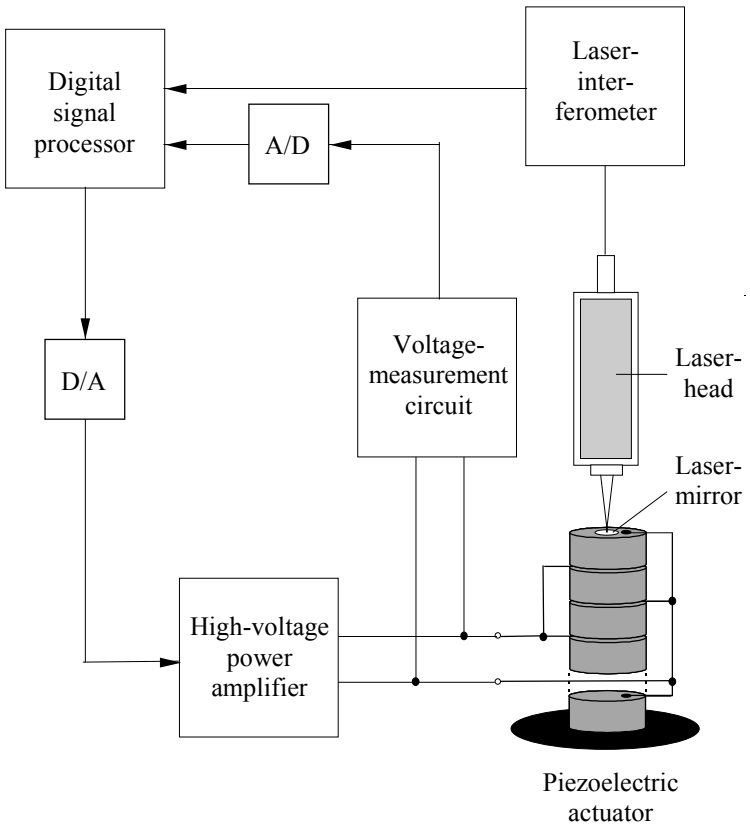
Digital signal processor
A/D
Laser-inter-ferometer
D/A
Voltage-measurement circuit
Laser-head
Laser-mirror
High-voltage power amplifier
Piezoelectric actuator

Fig.6